Adaptive Extended Kalman Filter for Integrated Navigation in a Satellite Launch Vehicle

Conference Paper · September 2022

DOI: 10.1109/ARGENCON55245.2022.9939949

3 authors:

Víctor Cánepa
Comisión Nacional de Actividades Espaciales

Pablo Servidia
Comisión Nacional de Actividades Espaciales

Juan I. Giribet
Universidad de San Andrés - CONICET

Adaptive Extended Kalman Filter for Integrated Navigation in a Satellite Launch Vehicle

Víctor Cánepa[+1], Pablo Servidia[+2], Juan Giribet[*]
[+]Navegación, Guiado y Control - Acceso al Espacio - Comisión Nacional de Actividades Espaciales,
Av. Paseo Colón 751, (1063) CABA, Argentina.
[+1] Email: *vcanepa@conae.gov.ar*
[+2] Email: *pservidia@conae.gov.ar*
[*]Departamento de Ingeniería, Universidad de San Andrés - CONICET
Vito Dumas 284, Victoria, Bs. As.
Email: *jgiribet@conicet.gov.ar*

Abstract – A flight navigation system usually integrates an Inertial Navigation System with a global positioning receiver by means of a Kalman Filter and using an appropriate model of the flight kinematics and the stochastic processes included on the inertial and external (global positioning by satellites) measurements. These processes are characterized mainly by their first and second order moments, the latter described by covariance matrices which can be time-varying. On a satellite launch vehicle the velocities are so high that the random delays of the external measurements generated by the receiver have a relevant effect on the navigation errors. This can be mitigated by an adaptive version of the Extended Kalman Filter, which is formulated in this work and verified by numerical simulations corresponding to an injection trajectory.

Resumen – En un sistema de navegación de vuelo que fusiona un sistema inercial con un receptor de posicionamiento global, el Filtro de Kalman necesita un modelo apropiado de la cinemática de vuelo en espacio de estados y de los procesos estocásticos que influyen en las mediciones inerciales y externas (posicionamiento global satelital). Estos procesos estocásticos se caracterizan principalmente mediante sus momentos de primer y segundo orden, estos últimos descriptos por matrices de covarianza que pueden variar con el tiempo. Para trayectorias de altas velocidades como un lanzador de satélites, el efecto en los retrasos en las mediciones GNSS tiene gran impacto en el error de navegación. Esto puede tratarse con una versión adaptativa del Filtro de Kalman Extendido, que se formula en este trabajo y finalmente se verifica mediante simulaciones numéricas en una trayectoria de inyección.

***Index Terms*—GNC Subsystem, Orbit Injection, Loosely-Coupled INS/GNSS, Adaptive Extended Kalman Filter.**

I. Introduction

A key tendency in the development of affordable modern navigation systems is the integration of an Inertial Navigation System (INS), which determines the kinematics using an Inertial Measurement Unit (IMU), and a receiver of a Global Navigation System by Satellites (GNSS); this is known as INS/GNSS integrated navigation. This Navigation output is fed-back at the inputs of the Guidance and Control, to be compared with the desired translation and attitude (i.e. rotation) of the vehicle as shown in Figure 1 ([1],[2],[3]).

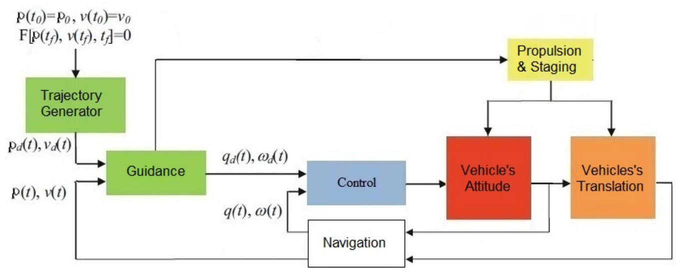

Fig. 1. Navigation, Guidance and Control Subsystem on an aerospace vehicle with propulsion.

The Extended Kalman Filter (EKF) is an efficient way to fuse information from different sources; it has been used since its formulation for the navigation of spacecraft. This filter requires to know the covariance matrices associated to the process noise (Q, related to inertial sensors and model uncertainties) and external measurements (R, related to the external measurements as given by a GNSS receiver).

On the previous implementation of the navigation algorithm on VEx vehicles in CONAE [4], [5], [6], the covariance matrices Q and R were considered constant, while the random GNSS measurements delays have been treated with a method good enough for a small suborbital rocket. However, a satellite launch vehicle as the Tronador II [1] must deal with high accelerations and high velocities, which determine a time varying uncertainty on the measurement delay effects. This can be handled by an adaptive version of an Extended Kalman Filter, which considers the available information on the measurement delay estimate to adapt the filter covariance associated to the external measurement. On the other hand, an adaptive version of the EKF, as proposed in [7], [8], is used to adapt the inertial measurement model by using the innovations sequence generated by the filter. A trade-off is made with respect to the current implementation used on VEx vehicles in CONAE, considering the increased complexity.

The next Section **II** presents the background of this work, including a summary of the kinematic model of the vehicle with measurements of inertial sensors (acceleration and angular velocity) and external GNSS receiver (translational

978-1-6654-8014-7/22/$31.00 ©2022 IEEE

position and velocity), presents the Extended Kalman Filter. Section **III** deals with the compensation of the delays on the external measurements proposing two methods: one based on the propagation of the external measurements, and the other on the propagation of the innovations which is the reference algorithm demonstrated in flight on the VEx vehicles in CONAE. The following section **IV** details a method for the adaptation of the process covariance using the innovations. These adaptive algorithms are implemented and evaluated by simulations in section **V**. Conclusions are given in section **VI**.

II. Background

A. Kinematics from inertial measurements

Let $\underline{x}(t)$ be the vector composed by the attitude, velocity and position coordinates of vehicle's body frame $\mathcal{B}$ respect to the Earth Centered Earth Fixed (ECEF) frame $\mathcal{E}$:

$$\underline{x} \quad := \quad \begin{bmatrix} \underline{\phi}^e_b \\ \underline{v}^e \\ \underline{p}^e \end{bmatrix} \tag{1}$$

where $\underline{\phi}^e_b \in \mathbb{R}^3$ represents the vector angle (Euler vector multiplied by the rotation angle) of the attitude of the body $\mathcal{B}$ respect to $\mathcal{E}$, $\underline{v}^e \in \mathbb{R}^3$ is the translational velocity and $\underline{p}^e \in \mathbb{R}^3$ the position on $\mathcal{E}$ frame. The kinematics coordinates are determined as a function of the angular velocity and the acceleration, therefore can also be given as a function of inertial measurements if the associated noises and the gravity model were known.

Let $\underline{\mu} := [\underline{\mu}_\omega^T \ \underline{\mu}_\mathrm{f}^T]^T$ be the vector of the angular velocity measurements $\underline{\mu}_\omega$ and the specific force $\underline{\mu}_\mathrm{f}$ (acceleration without gravity).

To complete the measurement description, a noise $\underline{\xi}_\omega$ is added to the angular velocity measurement, and a noise $\underline{\xi}_\mathrm{f}$ is added to the specific force measurement. The true gravity written in body frame and evaluated at the vehicle's position is $\underline{\gamma}^b + \underline{\xi}_g$, where $\underline{\xi}_g$ is a model uncertainty and $\underline{\gamma}^b$ is obtained from a gravity model $\underline{\gamma}^e$ in $\mathcal{E}$ frame, the vehicle's position $\underline{p}^e$, and the attitude matrix $\mathbf{C}^e_b$ as $\underline{\gamma}^b = \mathbf{C}^{e\,T}_b \underline{\gamma}^e(\underline{p}^e)$. The gravity model and the specific force measurements make possible to estimate the acceleration in body frame $\underline{a}^b$. The term $\underline{\xi}_g$ represents the model uncertainty of $\underline{\gamma}^b$ respect to the real gravity. Let $\underline{\xi}_\mu := [\underline{\xi}_\omega^T \ \underline{\xi}_\mathrm{f}^T \ \underline{\xi}_g^T]^T$. On the other hand, let $\underline{b} := [\underline{b}_\omega^T \ \underline{b}_\mathrm{f}^T]^T$ be the bias of angular velocity measurements $\underline{b}_\omega$ and specific forces bias $\underline{b}_\mathrm{f}$ which is modelled as a Markov processes, integrating random variables defined by $\underline{\xi}_b := [\underline{\xi}_{b\omega}^T \ \underline{\xi}_{b\mathrm{f}}^T]^T$, where $\underline{\xi}_{b\omega}$ and $\underline{\xi}_{b\mathrm{f}}$ are uncorrelated gaussian processes with zero mean. The IMU's measurement process can be described with the bias and noises model as:

$$\text{Measure}\left\{\underline{\omega}^b_{bi}, \underline{\xi}_\omega, \underline{b}_\omega(\underline{\xi}_{b\omega})\right\} \quad \longrightarrow \quad \underline{\mu}_\omega \tag{2}$$

$$\text{Measure}\left\{\underline{a}^b, \underline{\gamma}^b, \underline{\xi}_g, \underline{\xi}_\mathrm{f}, \underline{b}_\mathrm{f}(\underline{\xi}_{b\mathrm{f}})\right\} \quad \longrightarrow \quad \underline{\mu}_\mathrm{f} \tag{3}$$

where $\underline{\omega}^b_{bi}$ is the angular velocity of the vehicle in body frame. We can relate these quantities as:

$$\begin{cases} \dot{\underline{b}}_\omega &= \underline{\xi}_{b\omega} \\ \underline{\mu}_\omega &= \underline{b}_\omega + \underline{\omega}^b_{bi} + \underline{\xi}_\omega \\ \dot{\underline{b}}_\mathrm{f} &= \underline{\xi}_{b\mathrm{f}} \\ \underline{\mu}_\mathrm{f} &= \underline{b}_\mathrm{f} + \underline{a}^b - \underline{\gamma}^b - \underline{\xi}_g + \underline{\xi}_\mathrm{f} \end{cases} \tag{4}$$

where we consider the sensor frame as the body frame.

The following model relates the measurements with the kinematics [4]:

$$\begin{bmatrix} \dot{\underline{x}} \\ \dot{\underline{b}} \end{bmatrix} = \begin{bmatrix} f_\mu(\underline{x}, \underline{b}, \underline{\mu}) \\ \underline{\mathbf{0}} \end{bmatrix} + \begin{bmatrix} B_\mu(\underline{x}) & \mathbf{0}_{9\times6} \\ \mathbf{0}_{6\times9} & \mathbf{I}_{6\times6} \end{bmatrix} \begin{bmatrix} \underline{\xi}_\mu \\ \underline{\xi}_b \end{bmatrix} \tag{5}$$

where $\mathbf{0}_{n\times m}, \mathbf{I}_{n\times m} \in \mathbb{R}^{n\times m}$, $\underline{\mathbf{0}} \in \mathbb{R}^6$, f_μ maps the measurements and model parameters with the kinematic coordinates derivatives, and the matrix function B_μ transforms the measurement noises on their effects on the kinematics coordinates derivatives.

The vector of the process noises $\underline{\xi} := [\underline{\xi}_\mu^T \ \underline{\xi}_b^T]^T$, has zero mean and autocovariance:

$$C_{\xi\xi}(t,\tau) := \delta(\tau - t) Q^\xi(t) \tag{6}$$

where $\delta(\cdot)$ is the Dirac function [9]. We also define the augmented state vector $\underline{\chi} := [\underline{x}^T \ \underline{b}^T]^T$, hence the differential equation of $\underline{\chi}(t)$ is:

$$\dot{\underline{\chi}} = f(\underline{\chi}, \underline{\mu}) + B(\underline{\chi})\underline{\xi} \tag{7}$$

where:

$$f(\underline{\chi}, \underline{\mu}) \quad := \quad \begin{bmatrix} f_\mu(\underline{x}, \underline{b}, \underline{\mu}) \\ \underline{\mathbf{0}} \end{bmatrix} \tag{8}$$

$$B(\underline{\chi}) \quad := \quad \begin{bmatrix} B_\mu(\underline{x}) & \mathbf{0}_{9\times6} \\ \mathbf{0}_{6\times9} & \mathbf{I}_{6\times6} \end{bmatrix} \tag{9}$$

Following [4], we combine the specific force noise and gravity model uncertainty as an acceleration:

$$B_\mu(\underline{x}) := \begin{bmatrix} -\mathbf{I} & \mathbf{0} & \mathbf{0} \\ \mathbf{0} & -\mathbf{C}^e_b & \mathbf{I} \\ \mathbf{0} & \mathbf{0} & \mathbf{0} \end{bmatrix} \tag{10}$$

where $\mathbf{0} := \mathbf{0}_{3\times3}$ and $\mathbf{I} := \mathbf{I}_{3\times3}$.

B. Extended Kalman Filter

Let $\hat{\underline{\chi}}(t)$ be the estimation of the augmented state. We can linearize the associated dynamic model and describe the evolution of the error around the estimation, given by $\delta\underline{\chi} := \underline{\chi} - \hat{\underline{\chi}}$. The resulting system is linear time varying:

$$\delta\dot{\underline{\chi}} \approx F(\hat{\underline{\chi}}, \underline{\mu})\delta\underline{\chi} + B(\hat{\underline{\chi}})\underline{\xi} \tag{11}$$

with [9]:

$$F(\hat{\underline{\chi}}, \underline{\mu}) := \left.\frac{\partial f}{\partial \underline{\chi}}\right|_{\hat{\underline{\chi}}, \underline{\mu}} \tag{12}$$

$$= \begin{bmatrix} -\mathbf{S}(\hat{\underline{\omega}}^b_{bi}) & \mathbf{0} & \mathbf{0} & \mathbf{I} & \mathbf{0} \\ -\hat{\mathbf{C}}^e_b \mathbf{S}(\hat{\underline{\mathrm{f}}}^b) & -2\mathbf{S}(\underline{\mathbf{\Omega}}^e_{ei}) & \underline{\gamma}^e(\hat{\underline{p}}^e) & \mathbf{0} & \hat{\mathbf{C}}^e_b \\ \mathbf{0} & \mathbf{I} & \mathbf{0} & \mathbf{0} & \mathbf{0} \\ \mathbf{0} & \mathbf{0} & \mathbf{0} & \mathbf{0} & \mathbf{0} \\ \mathbf{0} & \mathbf{0} & \mathbf{0} & \mathbf{0} & \mathbf{0} \end{bmatrix}$$

where $\mathbf{S}(\underline{u})$ is the matrix associated to the vector product $\underline{u}\times$, the vector $\underline{\hat{f}}^b = \underline{\mu}_{\mathrm{f}} - \underline{\hat{b}}_{\mathrm{f}}$ is an estimate of the specific force as a function of the acceleration measured in body frame and the estimate $\underline{\hat{b}}_{\mathrm{f}}$ of the measurement bias, the vector $\underline{\hat{\omega}}_{bi}^b = \underline{\mu}_\omega - \underline{\hat{b}}_\omega$ is an estimate of the angular velocity in body frame as measured by the gyroscopes and compensated by the gyro bias estimation $\underline{\hat{b}}_\omega$, the matrix $\hat{\mathbf{C}}_b^e$ is an estimate of the attitude matrix and the vector $\underline{\mathbf{\Omega}}_{ei}^e$ is the Earth rotation velocity.

Let τ_k, with $k \in \mathbf{N}_0$, the discrete times on which there are external measurements from the receiver, such that $\tau_k = \tau_0 + k\triangle_\tau$. The augmented state error $\delta\chi_k := \delta\chi(\tau_k)$ verifies:

$$\begin{aligned} \delta\underline{\chi}_{k+1} &= \Phi(\tau_{k+1},\tau_k)\delta\underline{\chi}_k + \int_{\tau_k}^{\tau_{k+1}} \Phi(\tau_{k+1},s)B(s)\underline{\xi}(s)ds \\ &= \Phi(\tau_{k+1},\tau_k)\delta\underline{\chi}_k + \underline{\xi}_k^\chi \end{aligned} \tag{13}$$

where:

$$\underline{\xi}_k^\chi := \int_{\tau_k}^{\tau_{k+1}} \Phi(\tau_{k+1},s)B(s)\underline{\xi}(s)ds \tag{14}$$

is the discrete-time process zero-mean gaussian white-noise [10]. Its covariance matrix is given by [9]:

$$Q_k^\chi := \mathbf{E}[\underline{\xi}_k^\chi \underline{\xi}_k^{\chi T}] \tag{15}$$
$$\approx B_k Q_k^\xi B_k^T \triangle_\tau \tag{16}$$

where $B_k := B(\tau_k)$, Q_k^ξ is the covariance of the discretized noise[1], and $\triangle_\tau = \tau_{k+1} - \tau_k$. In the following, we will base our analysis on the discrete-time process noise vector $\underline{\xi}_k^\chi$ with covariance Q_k^χ.

On (13), the transition matrix for the state can be approximated by:

$$\Phi(\tau_{k+1},\tau_k) \approx \Phi_k := \exp(F(\underline{\hat{\chi}}_k, \underline{\mu}_k)\triangle_\tau) \tag{17}$$

where $F(\underline{\hat{\chi}}_k, \underline{\mu}_k)$ is computed with the estimate $\underline{\hat{\chi}}_k := \underline{\hat{\chi}}(\tau_k)$ based on the INS output at time τ_k and the inertial measurements $\underline{\mu}_k := \underline{\mu}(\tau_k)$, and the exponential function is approximated by a 5th-order polynomial.

Let $t_{k,n} = \tau_k + n\triangle_t$ be the times on which the INS outputs are generated, with $n = 0, 1, ..., N-1$ and $\triangle_t := \triangle_\tau / N$. One way to improve the computation of (17) is by factorization on N matrices:

$$\Phi(\tau_{k+1},\tau_k) \approx \Phi_{k,N-1} \,...\, \Phi_{k,1}\Phi_{k,0}, \tag{18}$$
$$\Phi_{k,n} := \exp(F(\underline{\hat{\chi}}_{k,n}, \underline{\mu}_{k,n})\triangle_t) \tag{19}$$

where $\underline{\mu}_{k,n}$ is the inertial measurement on $t_{k,n}$, $\underline{\hat{\chi}}_{k,n} := [\underline{\hat{x}}_{k,n}^T \ \underline{\hat{b}}_k^T]^T$, $\underline{\hat{x}}_{k,n}$ is the INS output on $t_{k,n}$ and $\underline{\hat{b}}_k$ is the estimated bias on τ_k. Note that $\underline{\hat{\chi}}_k = \underline{\hat{\chi}}_{k,0}$.

The discrete-time vector function $\underline{\tilde{y}}_k$ represents the external measurements from the GNSS receiver, with the position and velocity vectors in ECEF frame, evaluated at time τ_k. This can be written in terms of the augmented vector as:

$$\underline{\tilde{y}}_k := H\underline{\chi}_k + \underline{\eta}_k \tag{20}$$

where $\underline{\chi}_k := \underline{\chi}(\tau_k)$, $\underline{\eta}_k$ is a vector with the random noises of the external measurements, defined as a discrete-time gaussian and uncorrelated stochastic process, with zero mean and covariance matrix $R_k := \mathbf{E}[\underline{\eta}_k \underline{\eta}_k^T]$, and H is given as follows:

$$H := \begin{bmatrix} \mathbf{0} & \mathbf{0} & \mathbf{I} & \mathbf{0} & \mathbf{0} \\ \mathbf{0} & \mathbf{I} & \mathbf{0} & \mathbf{0} & \mathbf{0} \end{bmatrix} \tag{21}$$

The information available until $\tau_k > \tau_0$ is used to obtain the conditional expectation $\underline{\hat{\chi}}_k^k := \mathbf{E}[\underline{\chi}_k \,|\mathcal{M}_k,\, \mathrm{Y}_k^{\mathrm{GNSS}}]$ based on the set of inertial measurements $\mathcal{M}_k$ taken until τ_k, the set of external measurements $\mathrm{Y}_k^{\mathrm{GNSS}}$ given by the receiver until step k, and the covariance matrices as stated on the previous section. Therefore when a new measurement $\underline{\tilde{y}}_{k+1}$ arrives on time τ_{k+1}:

- The **prediction on** $k+1$ of the state as a function of the information taken until τ_k defines the estimate $\underline{\hat{\chi}}_{k+1}^k$.
- The **filter applied on** $k+1$ on the state and the new external measurement $\underline{\tilde{y}}_{k+1}$ generates the output $\underline{\hat{\chi}}_{k+1}^{k+1}$.

We also define $P_k^k := \mathbf{E}[\delta\underline{\chi}_k^k \delta\underline{\chi}_k^{k\,T}]$ where $\delta\underline{\chi}_k^k := \underline{\chi}_k - \underline{\hat{\chi}}_k^k$.

1) Prediction:
The prediction step on $k+1$ (*a priori* estimation considering external and inertial measurements until $k+1$) is defined as [10]:

$$\underline{\hat{\chi}}_{k+1}^k = \underline{\hat{\chi}}_{k,N-1} \tag{22}$$
$$P_{k+1}^k = \Phi_k \cdot P_k^k \cdot \Phi_k^T + Q_k^\chi \tag{23}$$

where $\underline{\hat{\chi}}_{k,N-1}$ is the output of the INS algorithm at τ_k, as given in [4], [9], and P_{k+1}^k is the covariance $\mathbf{E}[\delta\underline{\chi}_{k+1}^k \delta\underline{\chi}_{k+1}^{k\,T}]$. This recursive formula requires initialization for $k=0$ with the initial estimator $\underline{\hat{\chi}}_0^0 := \mathbf{E}[\underline{\chi}_0]$ and covariance P_0^0, using data from tests and other *a priori* information [11].

2) Filtering:
The estimator $\underline{\hat{\chi}}_{k+1}^{k+1}$ is based on the optimum linear filter (*a posteriori* estimation):

$$\underline{\hat{\chi}}_{k+1}^{k+1} = \underline{\hat{\chi}}_{k+1}^k + K_{k+1} \cdot \left(\underline{\tilde{y}}_{k+1} - \underline{\hat{y}}_{k+1}^k\right) \tag{24}$$

where $\underline{\hat{y}}_{k+1}^k := H\underline{\hat{\chi}}_{k+1}^k$ is the prediction of the external measurement from the receiver while K_{k+1} is the Kalman gain matrix computed after each new external measurement as:

$$K_{k+1} = P_{k+1}^k H^T \cdot \left(H \cdot P_{k+1}^k \cdot H^T + R_{k+1}\right)^{-1} \tag{25}$$

The covariance P_{k+1}^{k+1} is updated by:

$$P_{k+1}^{k+1} = P_{k+1}^k - K_{k+1} \cdot H \cdot P_{k+1}^k \tag{26}$$

C. Exponentially bounded EKF estimation error

In [12] it is shown that the discrete-time Extended Kalman Filter estimation error can be analysed in a stochastic framework with a nonlinear observability condition, which determines an exponentially bounded behaviour:

Definition 2.1: [12] The stochastic process $\underline{\chi}_k - \underline{\hat{\chi}}_k$ is said to be exponentially bounded in mean square when there are real numbers $a, b > 0$ and $0 < c < 1$ such that:

$$\mathbf{E}\left[\left\|\underline{\chi}_k - \underline{\hat{\chi}}_k\right\|^2\right] < a\left\|\underline{\chi}_0 - \underline{\hat{\chi}}_0^0\right\|^2 c^k + b \tag{27}$$

[1] We assume that it is pre-filtered to avoid alias and preserve de-correlation (see [9]).

holds for every $k \geq 0$.

To configure a sufficient condition for this behaviour, it is necessary to verify that there are $\underline{q}, \overline{q}, \underline{r}, \overline{r} > 0$ such that:

$$\underline{q} I \leq Q_k^{\chi} \leq \overline{q} I \tag{28}$$
$$\underline{r} I \leq R_k \leq \overline{r} I \tag{29}$$

The remaining conditions to guarantee exponentially boundedness are given in [12]. These conditions have been used to analyse the loosely coupled INS/GNSS implemented in CONAE's VEx-1 suborbital vehicle (see [13]).

III. Delayed GNSS measurements compensation

On each pulse per second (PPS) the receiver gets the information to compute the position and velocity, but this processing and packet transmission generates a random delay $\Delta t_k := \tau_k - t_{pps,k}$ to deliver the position and velocity external measures for the filter update. For the GNSS receiver under development [14], the packet data allows to obtain a measurement of the delay time $\tilde{\Delta} t_k$. In order to simplify this exposition, we consider only one GNSS constellation.

The following two subsections present methods to compensate these delays. On the first one, the measurement $\tilde{\Delta} t_k$ of this delay is used to compensate the external measurement in order to apply it to the filter as soon as possible. On the second one, a PPS signal is used to trigger the Kalman Filter update function on the next INS output slot, using the last external measurement delivered by the receiver. Notice that the first method uses the new information as soon as possible and does not require an additional electric signal, while the second one waits for the next PPS signal to implement the Kalman update step, hence the information is older when it is finally used.

A. Method 1: Compensation by measurements propagation

On each τ_k the navigation system applies the new external measurement on the filter, but this measurement actually corresponds to time $t_{pps,k} < \tau_k$ which implies a delay Δt_k. The position, velocity and delay becomes the GNSS receiver output variables (without noises):

$$\underline{y}_{pps,k} := \begin{bmatrix} \underline{p}_{pps,k}^{e\,T} & \underline{v}_{pps,k}^{e\,T} & \Delta t_k \end{bmatrix}^T \tag{30}$$

We propose to integrate one step by the Euler method to construct a new position/velocity output valid for τ_k:

$$H \underline{\chi}_k = \begin{bmatrix} \underline{p}^e(\tau_k) \\ \underline{v}^e(\tau_k) \end{bmatrix} = \underline{g}_k(\underline{y}_{pps,k}, \underline{a}_{pps,k}^e) + \underline{\varepsilon}_k \tag{31}$$

$$\text{with:} \quad \underline{g}_k(\underline{y}_{pps,k}, \underline{a}_{pps,k}^e) := \begin{bmatrix} \underline{p}_{pps,k}^e + \underline{v}_{pps,k}^e \Delta t_k \\ \underline{v}_{pps,k}^e + \underline{a}_{pps,k}^e \Delta t_k \end{bmatrix} \tag{32}$$

where $\underline{a}_{pps,k}^e := \underline{a}^e(t_{pps,k})$ is the acceleration in ECEF frame computed for $t_{pps,k}$. The propagation error $\underline{\varepsilon}_k$ is given as:

$$\underline{\varepsilon}_k(\underline{a}^e,\ \underline{\dot{a}}^e) \;:=\; \begin{bmatrix} \underline{a}^{e\,T}(\varsigma_1) & \underline{\dot{a}}^{e\,T}(\varsigma_2) \end{bmatrix}^T \cdot \frac{\Delta {t_k}^2}{2} \tag{33}$$

where $\underline{\dot{a}}^e$ is the derivative of $\underline{a}^e$ and $\varsigma_1, \varsigma_2 \in (t_{pps,k},\ \tau_k)$. The GNSS measurements will have noises:

$$\tilde{\underline{p}}_{pps,k}^e \;:=\; \underline{p}_{pps,k}^e + \underline{\eta}_{pk} \tag{34}$$
$$\tilde{\underline{v}}_{pps,k}^e \;:=\; \underline{v}_{pps,k}^e + \underline{\eta}_{vk} \tag{35}$$
$$\tilde{\Delta} t_k \;:=\; \Delta t_k + \eta_{\Delta t_k} \tag{36}$$

with $\underline{\eta}_{yk} := \begin{bmatrix} \underline{\eta}_{pk}^T & \underline{\eta}_{vk}^T & \eta_{\Delta t_k} \end{bmatrix}^T$ a gaussian zero-mean white-noise process with covariance $R_k^y := \mathbf{E}[\underline{\eta}_{yk} \underline{\eta}_{yk}^T]$. Moreover, we will consider an interpolator which estimates the velocity and acceleration using past INS data for $\tau_k - \tilde{\Delta} t_k \approx t_{pps,k}$. These variables are given as:

$$\hat{\underline{v}}_{pps,k}^e \;:=\; \underline{v}_{pps,k}^e + \underline{\eta}_{\hat{v}k} \tag{37}$$
$$\hat{\underline{a}}_{pps,k}^e \;:=\; \underline{a}_{pps,k}^e + \underline{\eta}_{\hat{a}k} \tag{38}$$

being $\underline{\eta}_{\hat{v}k}$ and $\underline{\eta}_{\hat{a}k}$ the velocity and acceleration estimation errors, modelled as gaussian zero-mean white-noise with covariances $R_k^{\hat{v}} := \mathbf{E}[\underline{\eta}_{\hat{v}k} \underline{\eta}_{\hat{v}k}^T]$ and $R_k^{\hat{a}} := \mathbf{E}[\underline{\eta}_{\hat{a}k} \underline{\eta}_{\hat{a}k}^T]$ respectively.

Using (34)-(38), we propose the compensated measurement:

$$\tilde{\underline{y}}_k := \begin{bmatrix} \tilde{\underline{p}}_{pps,k}^e + \hat{\underline{v}}_{pps,k}^e \tilde{\Delta} t_k \\ \tilde{\underline{v}}_{pps,k}^e + \hat{\underline{a}}_{pps,k}^e \tilde{\Delta} t_k \end{bmatrix} \tag{39}$$

and can be related with (31) as:

$$\tilde{\underline{y}}_k \;=\; \underline{g}_k(\underline{y}_{pps,k}, \underline{a}_{pps,k}^e) + \underline{\eta}_k \tag{40}$$

where $\underline{\eta}_k$ includes measurement noise, interpolation[2] and propagation errors. Neglecting $\underline{\eta}_{\hat{v}k} \eta_{\Delta t_k}$ and $\underline{\eta}_{\hat{a}k} \eta_{\Delta t_k}$ we have:

$$\underline{\eta}_k \;\approx\; \underline{\eta}_{pvk} + \underline{\eta}_{\hat{v}\hat{a}k} \Delta t_k + \underline{\dot{y}}_{pps,k} \eta_{\Delta t_k} + \underline{\varepsilon}_k \tag{41}$$

where $\underline{\eta}_{pvk} := [\underline{\eta}_{pk}^T \;\; \underline{\eta}_{vk}^T]^T$, $\underline{\eta}_{\hat{v}\hat{a}k} := [\underline{\eta}_{\hat{v}k}^T \;\; \underline{\eta}_{\hat{a}k}^T]^T$ and $\underline{\dot{y}}_{pps,k} := [\underline{v}_{pps,k}^{e\,T} \;\; \underline{a}_{pps,k}^{e\,T}]^T$. We will assume that every term in (41) is a random variable with zero-mean, orthogonal between each other, and with gaussian distributions. For the propagation error term $\underline{\varepsilon}_k$ this is a very conservative hypothesis which means that the attitude is assumed completely unknown, hence the acceleration vector in (33) has equal probability for every direcction, and therefore has zero mean (i.e. $\underline{\varepsilon}_k \in \mathcal{N}(\underline{0}, \underline{\varepsilon}_k^* \underline{\varepsilon}_k^{*T})$ for certain $\underline{\varepsilon}^*$ to be defined). The covariance matrix of compensated external measurement noises is:

$$\begin{aligned} R_k \;:=\; & \mathbf{E}[\underline{\eta}_{pvk} \underline{\eta}_{pvk}^T] + \mathbf{E}[\Delta {t_k}^2 \underline{\eta}_{\hat{v}\hat{a}k} \underline{\eta}_{\hat{v}\hat{a}k}^T] \;+ \\ & + \mathbf{E}[\eta_{\Delta t_k}^2] \underline{\dot{y}}_{pps,k} \underline{\dot{y}}_{pps,k}^T + \mathbf{E}[\underline{\varepsilon}_k \underline{\varepsilon}_k^T] \end{aligned} \tag{42}$$

An estimate of R_k is given as:

$$\hat{R}_k \;= \hat{R}_k^{pv} + \tilde{\Delta} {t_k}^2 \cdot \hat{R}_k^{\hat{v}\hat{a}} + \hat{\sigma}_{\eta_{\Delta t}}^2 \hat{\underline{\dot{y}}}_{pps,k} \hat{\underline{\dot{y}}}_{pps,k}^T + \underline{\varepsilon}_k^* \underline{\varepsilon}_k^{*\,T} \tag{43}$$

where $\hat{\underline{\dot{y}}}_{pps,k} := [\hat{\underline{v}}_{pps,k}^{e\,T} \;\; \hat{\underline{a}}_{pps,k}^{e\,T}]^T$ is the interpolator output, $\hat{\sigma}_{\eta_{\Delta t}}^2$ an estimate of $\sigma_{\eta_{\Delta t_k}}^2$ and:

$$\underline{\varepsilon}_k^* \;:=\; \begin{bmatrix} \hat{\underline{a}}_{pps,k}^{e\,T} & \frac{\hat{\underline{a}}_{pps,k}^{e\,T} - \hat{\underline{a}}_{pps,k-1}^{e\,T}}{\Delta_\tau} \end{bmatrix}^T \cdot \frac{\tilde{\Delta} {t_k}^2}{2} \tag{44}$$

$$\hat{R}_k^{\hat{v}\hat{a}} \;:=\; \begin{bmatrix} \hat{R}_k^{\hat{v}} & \mathbf{0} \\ \mathbf{0} & \hat{R}_k^{\hat{a}} \end{bmatrix}$$

[2] This makes the process and measurement noises slightly correlated, but may be considered negligible for the velocities of the orbital injection trajectory.

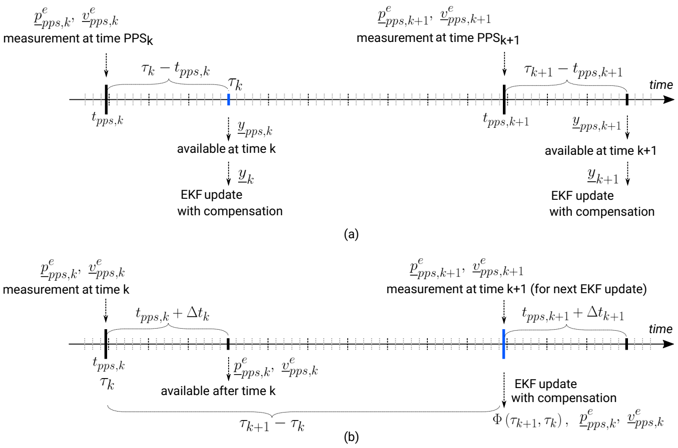

Fig. 2. Data flow diagram for each delay compensation: method 1 (a) is based on measurement propagation, and method 2 (b) is based on innovations propagation. The EKF update times are shown in blue.

The covariance $\hat{R}_k^{pv}$ is determined by the receiver, while $\hat{R}_k^{\hat{v}\hat{a}}$ is determined by the interpolator.

The Figure 2-(a) summarizes this compensation scheme, while the Figure 3 shows the implementation architecture. The innovation is computed using (40) as:

$$\delta \underline{y}_k \quad = \quad \tilde{\underline{y}}_k - H \hat{\underline{\chi}}_k^{k-1} \tag{45}$$

Remark *3.1:* The velocity is part of the state $\underline{\chi}_k$, hence we have an estimate of the covariance for the INS outputs and this allows to estimate the covariance of the interpolated values $\hat{R}_k^{\hat{v}}$. However, there is no covariance estimate for the acceleration. To compute $\hat{R}_k^{\hat{a}}$, we use the estimation of $\hat{R}_k^{\hat{v}}$:

$$\begin{aligned} \underline{\eta}_{\hat{a}k} &= \hat{\underline{a}}_{pps,k}^e - \underline{a}_{pps,k}^e \\ &\approx \frac{\hat{\underline{v}}_{pps,k}^e - \hat{\underline{v}}_{pps,k-1}^e}{\Delta_\tau} - \frac{(\underline{v}_{pps,k}^e - \underline{v}_{pps,k-1}^e)}{\Delta_\tau} \\ &= \frac{\underline{\eta}_{\hat{v}k} - \underline{\eta}_{\hat{v}k-1}}{\Delta_\tau} \end{aligned} \tag{46}$$

and considering that $\mathbf{E}[\underline{\eta}_{\hat{v}k} \underline{\eta}_{\hat{v}k-1}^T] = \mathbf{0}$ we obtain:

$$\begin{aligned} \mathbf{E}[\underline{\eta}_{\hat{a}k} \underline{\eta}_{\hat{a}k}^T] &\approx \frac{1}{\Delta_\tau^2} \mathbf{E}[(\underline{\eta}_{\hat{v}k} - \underline{\eta}_{\hat{v}k-1})(\underline{\eta}_{\hat{v}k} - \underline{\eta}_{\hat{v}k-1})^T] \\ &= \frac{1}{\Delta_\tau^2} \left(\mathbf{E}[\underline{\eta}_{\hat{v}k} \underline{\eta}_{\hat{v}k}^T] + \mathbf{E}[\underline{\eta}_{\hat{v}k-1} \underline{\eta}_{\hat{v}k-1}^T] \right) \\ &\approx \frac{2}{\Delta_\tau^2} \cdot \mathbf{E}[\underline{\eta}_{\hat{v}k} \underline{\eta}_{\hat{v}k}^T] \end{aligned} \tag{47}$$

B. Method 2: Compensation by corrections propagation

Following [4], an alternative method is based on the propagation of the correction process. This method makes the updates on the PPS times which are assumed to be reported in the receiver data, or detected from a separate PPS signal. The position and velocity measurements are again available at $\tau_k = t_{pps,k} + \Delta t_k$, but on this method the EKF is not updated immediately. Instead, the external measurement is stored until the next PPS is detected, at $t_{pps,k+1}$, and the update is made by using the stored data. Hence this method may be more useful when Δt_k is near one second; otherwise there will be a degradation because the stored information becomes older when it is finally used. On the applications where the velocities and accelerations are small, a delay around 500 ms has been compensated [5] with flight demonstrations made on VEx vehicles. To this end, the correction must be propagated in order to be able to upgrade the current state:

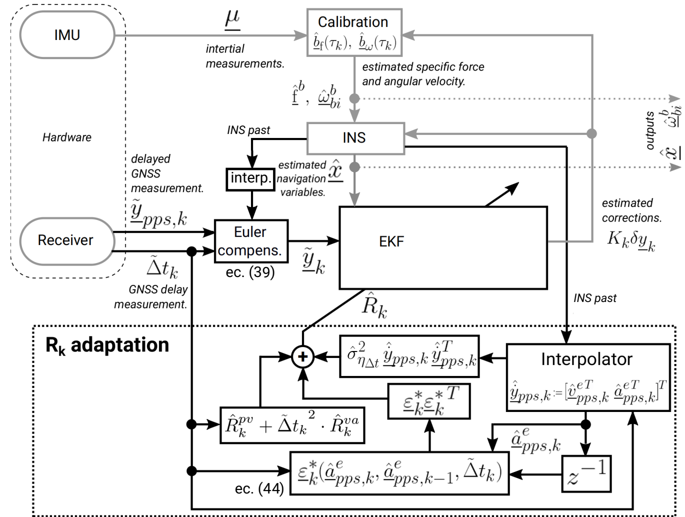

Fig. 3. Block diagram of INS/GNSS implementation, with adaptation of R_k, delay compensation by Euler method and the interpolator data INS for $t_{pps,k}$. The vector $\tilde{\underline{y}}_{pps,k}$ is a measurement of (30).

$$\delta \hat{\underline{\chi}}_{k+1}^k = \Phi_k \cdot K_k \cdot \delta \underline{y}_k \tag{48}$$

where $\delta \underline{y}_k := \tilde{\underline{y}}_{pps,k} - H \hat{\underline{\chi}}_k^{k-1}$ with $\tilde{\underline{y}}_{pps,k} := [\tilde{\underline{p}}_{pps,k}^{e\,T} \; \tilde{\underline{v}}_{pps,k}^{e\,T}]^T$ for this method.

IV. Adaptation of Q_k^χ with innovations

In this section we deal with other possible time-varying effects without an specific structure as the measurements delay. Following [7], we propose an estimator of the covariance Q_k^χ using the innovations. Taking $\underline{\xi}_k^\chi$ from (13):

$$\begin{aligned} \underline{\xi}_k^\chi &= \delta \underline{\chi}_{k+1} - \Phi(\tau_{k+1}, \tau_k) \delta \underline{\chi}_k \\ &= \underline{\chi}_{k+1} - \hat{\underline{\chi}}_{k+1} - \Phi(\tau_{k+1}, \tau_k) \underline{\chi}_k + \Phi(\tau_{k+1}, \tau_k) \hat{\underline{\chi}}_k \\ &\approx -\hat{\underline{\chi}}_{k+1} + \Phi(\tau_{k+1}, \tau_k) \hat{\underline{\chi}}_k \end{aligned} \tag{49}$$

where we have used $\underline{\chi}_{k+1} \approx \Phi(\tau_{k+1}, \tau_k) \underline{\chi}_k$.

Let $\overline{\Phi}_k$ be an approximation of $\Phi(\tau_{k+1}, \tau_k)$ computed with (17) or (18). We estimate $\hat{\underline{\chi}}_k$ with $\hat{\underline{\chi}}_k^k$ while $\hat{\underline{\chi}}_{k+1}$ is estimated by $\hat{\underline{\chi}}_{k+1}^{k+1}$ obtained from (24). Hence we obtain:

$$\underline{\xi}_k^\chi \quad \approx \quad -\hat{\underline{\chi}}_{k+1}^{k+1} + \overline{\Phi}_k \hat{\underline{\chi}}_k^k \tag{50}$$

$$\approx \quad -K_k \delta \underline{y}_k \tag{51}$$

where $\delta \underline{y}_k := \tilde{\underline{y}}_k - \underline{h}_k(\hat{\underline{\chi}}_k^{k-1})$. The covariance $Q_k^\chi = \mathbf{E}[\underline{\xi}_k \underline{\xi}_k^T]$ can be approximated by:

$$Q_k^\chi \quad \approx \quad \mathbf{E}[K_k \delta \underline{y}_k \delta \underline{y}_k^T K_k^T] \tag{52}$$

using the average on a window with length L:

$$\hat{Q}_{L,k}^y \quad = \quad \frac{1}{L} \sum_{j=k+1-L}^{k} K_j \delta \underline{y}_j \delta \underline{y}_j^T K_j^T \tag{53}$$

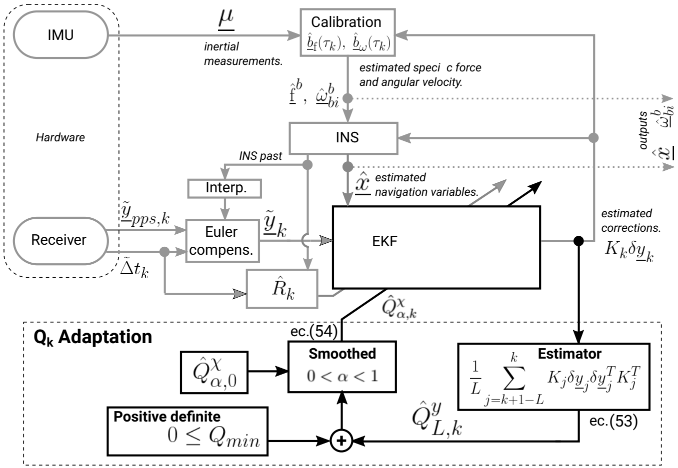

Fig. 4. Proposed implementation for the estimation of Q^χ_k.

A. Smooth positive definite estimator

The moving average $\hat{Q}^y_{L,k}$ in (53) is only guaranteed semi-positive definite, hence we propose a positive definite estimator using a a lower bound $0 \le Q_{min} \in \mathbb{R}^{15\times15}$, and a smoothing factor $0 < \alpha < 1$:

$$\hat{Q}^\chi_{\alpha,k} = \alpha\hat{Q}^\chi_{\alpha,k-1} + (1-\alpha)\left(Q_{min} + \hat{Q}^y_{L,k}\right) \quad (54)$$

The implementation in shown in Figure 4. For $k = 0$, we will use $\hat{Q}^\chi_{\alpha,0} \ge Q_{min}$, which guarantees the positive-definiteness of the estimator:

$$\hat{Q}^\chi_{\alpha,k} = \alpha\hat{Q}^\chi_{\alpha,k-1} + (1-\alpha)Q_{min} + (1-\alpha)\hat{Q}^y_{L,k} \quad (55)$$

where the first two terms are positive-definite by construction and the last one is semi-positive definite, which guarantees $\hat{Q}^\chi_{\alpha,k} > 0$. In particular, for $\hat{Q}^\chi_{\alpha,0} = Q_{min}$ we obtain:

$$\hat{Q}^\chi_{\alpha,k} = Q_{min} + (1-\alpha)\sum_{j=1}^{k}\alpha^{k-j}\hat{Q}^y_{L,j} \quad (56)$$

which implies $\hat{Q}^\chi_{\alpha,k} \ge Q_{min} > 0$ for all k, as required for (28). A time-varying $Q_{min,k}$ may also be used on (55) for $Q_{min,k} > Q_{min} > 0$, but (56) would not hold.

V. Simulation results

Here we verify the performance of the proposed adaptations on the Extended Kalman Filter for a satellite launcher injection trajectory on Low Earth Orbits (LEO). The simulation considers a two stage vehicle with maximum accelerations around 6 g and injection altitude of 350 km, with a typical trajectory as shown in Figure 5. For all the simulations, the vehicle is static on the launch platform the first minute, which is the lift-off time. The injection velocity is attained at after 10 minutes from the simulation start. The upper trace shows the altitude (blue) in kilometers and the acceleration (red) in meters per square second. The lower trace shows in blue the ECEF velocity norm in kilometers per second (blue) and the angular velocity as measured by the IMU in degrees per seconds (red).

Following the acceleration profile we can see at the first minute corresponding to the lift-off. Before four minutes can be seen the main engine cut-off of the first stage, followed by the separation and ignition event of the second stage, whose engine cut-off is made after 10 minutes from simulation start.

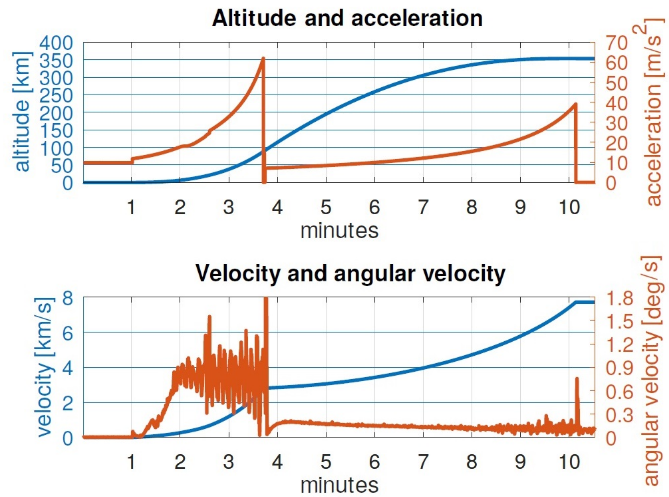

Fig. 5. The upper plot shows in blue the navigated altitude of the vehicle respect to the launch site level, and in red the norm of the acceleration as measured by the Inertial Measurement Unit (IMU). The lower plot shows in blue the norm of the navigated velocity in ECEF frame and in red the norm of the angular velocity as measured by the IMU.

A. Availability of GNSS satellites during ascent

A numerical simulation tool was developed to model the GNSS satellites and the receiver behaviour, as shown in [1]. The integrated navigator proposed here was tested with a model of a GPS-L1 GLONASS-L1 receiver. Figure 6 shows the number of tracked GNSS satellites considering the processing behaviour of the receiver's state machine as well as the geometry of the L-band antennas of vehicle and satellites. This includes a model on the radiation pattern of the antennas in the link, the free space losses, and the minimum sensitivity of the receiver respect to the noise, modelled as a minimum signal to noise ratio C/N_0. On the Figure 7 we show a sky zenith view of the GNSS satellites as seen during the flight, in elevation/acimuth coordinates. During the ascent, new satellites are incorporated to the solution computation due to the increased height, and also some satellites are lost due to the relative movement respect the horizon. The initial satellites as seen from the launch site are indicated with black circles.

The delay of the receiver depends on the number of satellites to be processed, which can be modelled by the numerical simulations as shown here and will be validated using hardware in the loop simulations on the GSS8000 Spirent simulator available on the NGC laboratory at CONAE headquarters.

B. EKF update delays compensation

In order to make a fair comparison between both compensation methods, a constant delay of 900 ms is simulated first on the GNSS receiver measurements. On both methods we have considered that the estimated delay is one second with a discrepancy of -100 ms on the delay knowledge. Figure 8 shows

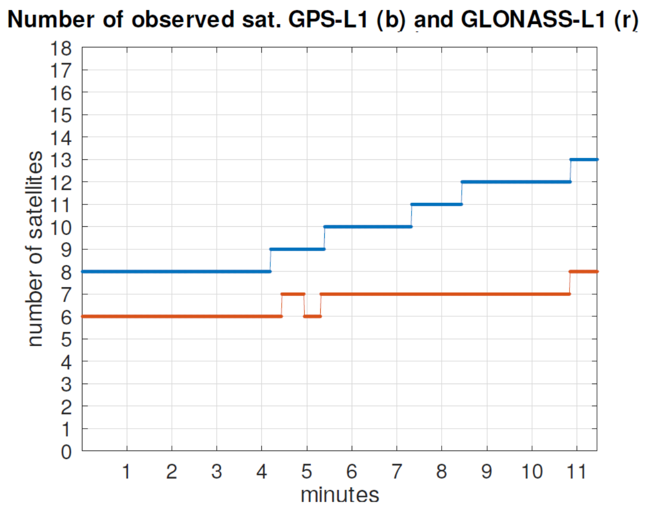

Fig. 6. Number of GNSS satellites tracked by the receiver; in blue GPS-L1 and in red GLONASS-L1.

the logarithm of the norm of the estimation errors in attitude, position and velocity. The black trace shows the result without delay as a reference. The result with both adaptive methods (green for corrections propagation and blue for measurement propagation by Euler) have better performance compared with the case without compensation (in red). We consider that even in this case with a delay around one second there is an advantage for the Euler compensation method as it does not require the PPS signal synchronization while minimizes the latency of the updates in the case that the delays were variable and smaller.

C. Compensation for delays $\Delta t_k \ll 1$ sec

As previously mentioned, when the delay is negligible with respect to one second, the correction propagation method will have a latency around one second, i.e. $1\text{sec} - \Delta t_k$, for the EKF update. Under fast and variable dynamics, as is the case of a satellite launch vehicle, this determine a degradation of the estimation error.

Instead, the method based on the propagation of the measurement makes possible an immediate implementation of the update, hence the latency is minimized. Figure 9 shows the result with a constant delay of $\Delta t_k = \tilde{\Delta} t_k = \hat{\Delta} t_k = 300$ ms comparing the errors on cases without compensation (in red trace), with Euler compensation (in blue trace) and without delay (in black, as a reference). The new GNSS receivers developed for this project [15], [14] fits this delay model even with smaller delays than the 300 ms value taken here as a worst case simulation.

D. Adaptation of the process noise covariance Q_k^χ

We compare now the performance of the Extended Kalman Filter with and without adaptation on the process noise covariance Q_k^χ. The delay was also taken as 300 ms. The adaptation uses the implementation as shown in Figure 4 with $\alpha = 0.99$ and $L = 1$, using (53) and (54).

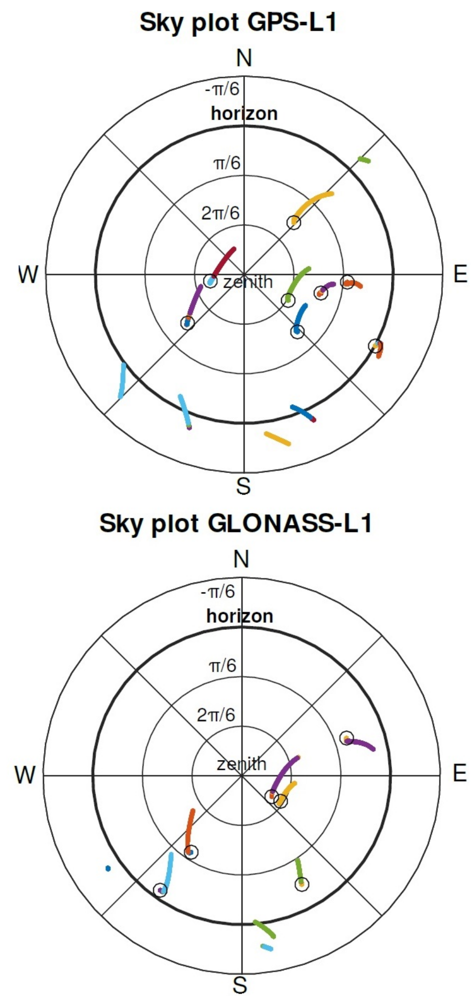

Fig. 7. Local sky azimuth and elevation for each satellite tracked by the receiver.

The Figure 10 shows the logarithm of the norm of the estimation error in position. The green trace shows the case without adaptation, having a larger estimation error compared to the smooth adaptive algorithm with $Q_{min} = Q_{\alpha,0}^\chi > 0$ in red and $Q_{min} = Q_{\alpha,0}^\chi = \mathbf{0}_{15\times15}$ in black.

From these results we can see that the adaptive algorithm shows an improvement respect to a constant Q which has to be weighted against the increased complexity.

VI. Conclusions

We have evaluated improvements on the integrated navigation algorithm used on VEx vehicles:

- Adaptation of R for delayed GNSS measurements compensation by Euler propagation.
- Adaptation of Q using a smooth estimator based on innovations.
- Factorization of the transition matrix.
- Simulation of a realistic satellite injection trajectory.

This results show that the delay compensation through Euler propagation of external measurements is more convenient than the previous method for the GNSS receiver under consideration, which justifies this new implementation. The adaptation

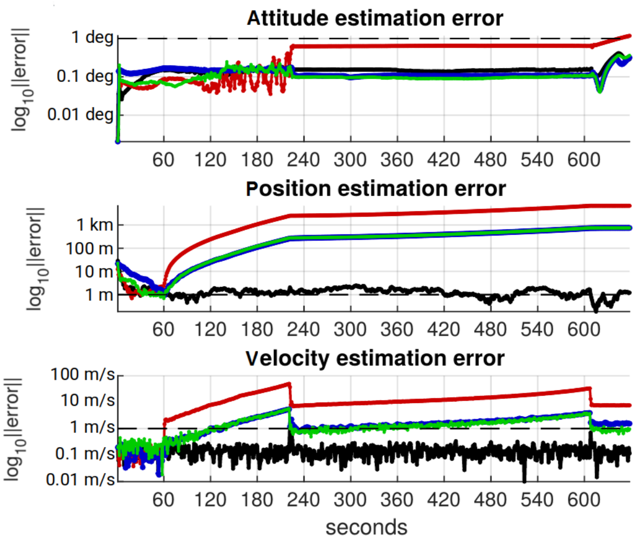

Fig. 8. Logarithm of the norm of the estimation errors of attitude, position and velocity for a delay of 900 ms without compensation (red), with Euler compensation of 1000 ms (blue), by propagation of corrections (green) and without delay (in black, as reference).

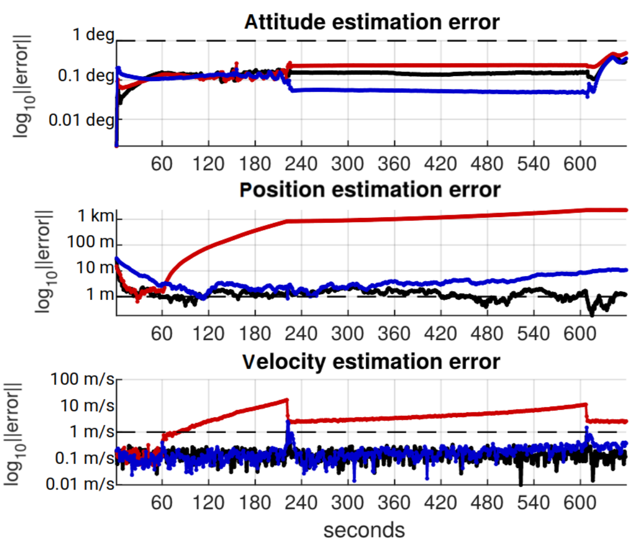

Fig. 9. Logarithm of the norm of the estimation errors of attitude, position and velocity for a delay of 300 ms without compensation (red), with Euler compensation (blue) and without delay (in black, as a reference).

of Q did not show good enough results to balance the increased complexity of the implementation. Moreover, the factorization of the transition matrix did not show improvements to consider this implementation.

As future work we will implement a tightly coupled integration of GNSS measurements to improve the estimation of inertial sensor bias in flight, but the current results are good enough for attitude, velocity and position estimation for the NGC subsystem of a satellite launcher.

VII. Acknowledgements

This work was made at the Comisión Nacional de Actividades Espaciales (CONAE), which depends on the Ministerio de Ciencia, Tecnología e Innovación Productiva de Argentina, with participation of the LAR group on the Facultad de Ingeniería de la Universidad de Buenos Aires (FIUBA). We also acknowledge helpful discussions with Dr. Martin España in CONAE, and the collaboration of the SENYT group on the Universidad Nacional de La Plata (UNLP).

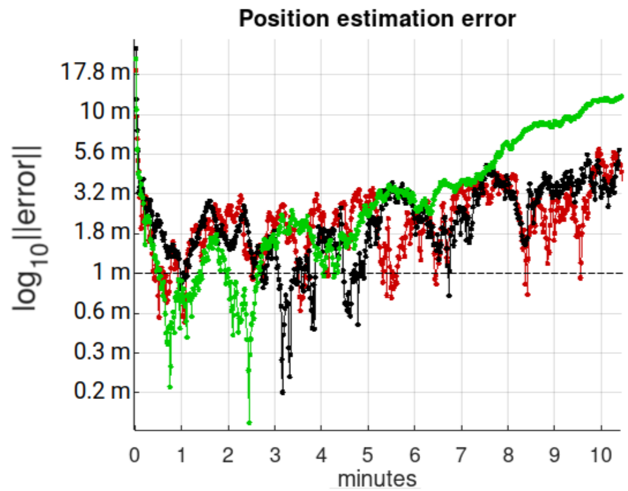

Fig. 10. Logarithm of the norm of estimation error in position for a delay of 300 ms on receiver updates with Euler compensation. The green traces shows the EKF result with constant Q, the red traces the EKF with adaptive Q using (54) and the black trace shows the same adaptive case making zero the Q_{min} matrix parameter. On both adaptive cases we have used $\alpha = 0.99$ and $L = 1$.

References

[1] Moreno, A., Canepa, V., Giribet, J., Servidia, P., *Simulador GNSS para la Evaluación de Algoritmos de Navegación Intergada en Vehículos Aeroespaciales*. Proceedings of the Congreso Argentino de Tecnología Espacial, CATE-2021.

[2] Tewari A, *Advanced Control of Aircraft, Spacecraft and Rockets*, Wiley, 2011.

[3] Suresh B.,Sivan K., *Integrated Design for Space Transportation Systems*, Springer, 2015.

[4] Bernadi P., *Sistema de Navegación INS/GPS para un Cohete Suborbital Controlado*, University of Buenos Aires. 2013.

[5] Servidia, P., *Propuesta y análisis de leyes de Guiado y Control para el VEx1*, PDR-VEx1, CONAE, 2011.

[6] Servidia P., *TT3-030201-RQ-00100-F - Requisitos L3 del Subsistema de NGCT*, CONAE, 2018.

[7] Akhlaghi, S., Zhou, N., Huang, Z., *Adaptive Adjustment of Noise Covariance in Kalman Filter for Dynamic State Estimation*. IEEE Power and Energy Society General Meeting. July 2017.

[8] Zhang, L., Wang, S., Seleneva, M. S., Neusypin, K. A., *A new Adaptive Kalman filter for navigation systems of carrier-based aircraft*, Chinese Journal of aeronautics, 2021.

[9] España, M., *Sistemas de Navegación Integrada con Aplicaciones (2^a Edición 2019)*, Comisión Nacional de Actividades Espaciales, *www.argentina.gob.ar/ciencia/conae/publicaciones*.

[10] Jazwinski, A, H., *Stochastic Processes and Filtering Theory*. Mathematics in Science and Engineering. Vol. 64. 1970.

[11] Bernadi, P., Giribet, J., Servidia, P., *Algoritmo de alineación para el VEx-1*, CONAE-FIUBA. 2013.

[12] Reif, K., Günther, S., Yaz, E., *Stochastic stability of the discrete-time Extended Kalman Filter*, IEEE, Vol. 44, No 4, April 1999.

[13] Roasio, F., Giribet, J., Servidia, P., *Análisis de estabilidad del Filtro de Kalman Extendido del sistema de navegación del VEx1*, CONAE-FIUBA. 2013.

[14] T2A-17.21.02.00-ME-0001-A *Memo de actualizaciones de software de los receptores M3GR*, SENYT-UNLP, contract VENG-CTA, 2021-2022.

[15] Lopez La Valle, R., Rodriguez, S., Garcia, J., *Documento de Control de Interfaces M3GR-EMB*, SENYT-UNLP, 2018.